NANO LETTERS

2007
Vol. 7, No. 8
2227−2233

Transition from Two-Dimensional to Three-Dimensional Quantum Confinement in Semiconductor Quantum Wires/Quantum Dots

Q. Zhu,* K. F. Karlsson, E. Pelucchi,† and E. Kapon

Laboratory of Physics and Nanostructures, Ecole Polytechnique Fédérale de Lausanne (EPFL), CH-1015 Lausanne, Switzerland

Received March 21, 2007; Revised Manuscript Received June 4, 2007

ABSTRACT

We report the photoluminescence (PL) and polarization-resolved PL characteristics of a novel GaAs/AlGaAs quantum wire/dot semiconductor system, realized by metalorganic vapor-phase epitaxy of site-controlled, self-assembled nanostructures in inverted tetrahedral pyramids. By systematically changing the length of the quantum wires, we implement a continuous transition between the regimes of two-dimensional and three-dimensional quantum confinement. The two main evidences for this transition are observed experimentally and confirmed theoretically: (i) strongly blue-shifted ground-state emission, accompanied by increase separation of ground and excited transition energies; and (ii) change in the orientation of the main axis of linear polarization of the photoluminescence, from parallel to perpendicular with respect to the wire axis. This latter effect, whose origin is shown to be purely due to quantum confinement and valence band mixing, sets in at wire lengths of only ∼30 nm.

The electronic structure of quantum wires (QWRs) and quantum dots (QDs) has been extensively investigated in different semiconductor structures, revealing many features characteristic of two-dimensionally (2D) and 3D confined systems.[1] Many optical features of these low-dimensional structures, for example, polarization anisotropy,[2] exciton lifetime,[3] binding energies of excitons and exciton complexes,[4] and other many-body effects,[5,6] depend crucially on the dimensionality of the system. A useful way of examining the effect of dimensionality in these systems would be to consider a QWR of finite length and then to explore the modifications in its optical properties as its length is decreased. Concerning quantum confinement effects, one can distinguish between two QWR length scales. For finite-length QWRs that are long enough such that only the center-of-mass motion of excitons is quantized ("weak" 3D confinement), the impact of quantum confinement on the carrier envelope functions is negligible. For QWR lengths comparable to the exciton Bohr diameter ("strong" 3D confinement), more fundamental effects such as modified exciton life time and valence band mixing are expected to take place. Such nanostructures of "tailored dimensionality" would also be interesting for constructing mixed-dimensionality systems, for example, QD molecules and superlattices coupled by QWR segments.

In real QWR structures, potential disorder may induce carrier localization into QD-like sections with slightly different confining potentials.[5,7] Certain features of exciton localization, for example, luminescence spectra exhibiting QD-like, sharp features at low temperatures, have been observed in such disordered wires.[5,7] Transition between QD-like and QWR-like excitonic features have been assigned to such structures incorporating 50 nm long QD-segments at 10 K.[8] In general, however, disordered QWRs exhibit random localization potential profiles, which do not make them suitable for elucidating the transition from a 1D (QWR) to a 0D (QD) structure in a systematic way.

Such an investigation requires a model system in which the dimensionality of the nanostructure can be controlled in a sufficiently fine and reproducible manner. Several techniques in which both QWRs and QDs can be realized in the very same low-dimensional system have been explored and developed, including cleaved-edge overgrowth of T-shaped QWRs and QDs,[9] core−shell nanowires and dots grown by catalyzed metallorganic chemical vapor deposition (MOVPE),[10] and pyramidal QWRs/QDs grown by MOVPE on patterned substrates.[11,12] The latter approach is particularly attractive because it offers both control of the QWR heterostructure potential along its axis and, simultaneously, results in site-

* To whom correspondence should be addressed. E-mail: qing.zhu@epfl.ch.

† Current address: Tyndall National Institute, "LeeMaltings", Prospect Row, Cork, Ireland.

10.1021/nl0706650 CCC: $37.00
Published on Web 07/11/2007

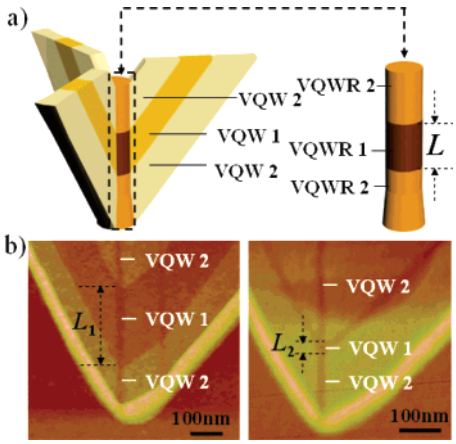

Figure 1. (a) Schematic illustration of the nanostructures formed inside the inverted pyramid, including AlGaAs VQWR1,2 and VQW1,2 (left panel); simplified illustration of the VQWR heterostructure in the center of the pyramid (right panel). (b) Flattened cross-sectional AFM images of pyramidal heterostructures containing 300 nm (left panel) and 24 nm (right panel) thick VQW1; the lowest, bright layer represents the thin $Al_{0.75}Ga_{0.25}As$ etch-stop sacrificial layer.

controlled, embedded QWR/QD structures of high optical quality, amenable for luminescence studies.

Here we report the characteristics of a length-controlled QWR/QD system, self-formed during MOVPE of GaAs/AlGaAs heterostructures in inverted tetrahedral pyramids.[12] Because of strong Ga−Al segregation effects, driven by capillarity fluxes generated at the highly curved wedges and tip of the pyramid, three Ga-enriched AlGaAs vertical quantum wells (VQWs) are formed at the wedges of the pyramid, meeting at the center to form a Ga-enriched AlGaAs vertical QWR (VQWR) running through the center of the pyramid (see Figure 1a). Most importantly, the wire axis is formed along the growth direction. Thus, simply by adjusting the growth parameters (e.g., layer thicknesses, Al and/or Ga fluxes, surface temperature, etc.) the length, width, and composition of the wire can be controlled flexibly and precisely. In particular, it is possible to systematically shorten the length of the QWR all the way into the nanometer range forming a QD while keeping other parameters unchanged. Using low-temperature photoluminescence (PL) spectroscopy and numerical modeling, we study systematically the electronic transitions in these structures and identify the characteristic lengths of the QWRs for which features signifying 3D quantum confinement appear.

A series of samples consisting of $Al_{0.3}Ga_{0.7}As$ VQWR layers sandwiched between $Al_{0.55}Ga_{0.45}As$-cladding layers were grown on 2°-off-(111)B GaAs substrates patterned with 5 μm pitch arrays of inverted tetrahedral pyramids exposing {111}A facets.[11] The substrates were prepatterned by photolithography and wet chemical etching. The MOVPE growth was performed at low pressure (20 mb) in nitrogen atmosphere at a substrate temperature of 665 °C and V/III ratio of 500. All investigated samples had nominally identical structure, except that the thickness of the $Al_{0.3}Ga_{0.7}As$ VQWR core layer was varied systematically from sample to sample (see below for further details). In all structures, a thin $Al_{0.75}Ga_{0.25}As$ etch-stop layer was grown between the GaAs substrate and the $Al_{0.3}Ga_{0.7}As/Al_{0.55}Ga_{0.45}As$ heterostructure to help in subsequent substrate removal.[11]

Growth of an AlGaAs of given nominal composition yields three distinct phases, formed due to capillarity-induced Al−Ga segregation at the wedges and the tip of the inverted pyramid. Schematic illustration of the grown structure is shown in Figure 1a, left panel, in which the brown scale represents the Al concentration in the corresponding region. The darkest parts at the center of the pyramid correspond to the VQWRs formed at the tip, where the capillarity-induced adatom fluxes are strongest and hence the Al content is the lowest. In the particular structures studies, a lower Al-content wire, designated VQWR1, is formed in the $Al_{0.3}Ga_{0.7}As$ layer and is bounded below and above by higher Al-content wires, VQWR2, formed in the $Al_{0.55}Ga_{0.45}As$-cladding layers. VQWR1 thus defines a lower potential QWR inserted between higher potential QWRs. The weaker capillarity-induced adatom fluxes at the wedges of the pyramids yield AlGaAs VQWs that have higher Al contents than the corresponding VQWR regions but lower than that of the corresponding bulk AlGaAs regions (see Figure 1a). The lowest band gap (lowest Al content) regions of the pyramidal heterostructure consist thus of a VQWR segment of specific length L clad by two, higher band gap VQWRs, as schematically shown in Figure 1a, right panel. The length of the VQWR segment is directly determined by the growth time of the lower-Al-content AlGaAs layer. Its composition and width can be tuned by adjusting the growth conditions (rate, temperature, V/III ratio, etc.) of the corresponding layer. Moreover, its potential barriers can be adjusted by proper design of the clad VQWR regions and/or the composition of the VQWs.

The grown samples were structurally characterized using cross-sectional atomic force microscopy (AFM) in air ambiance. Figure 1b shows representative AFM cross sections of two of the grown samples. The contrast in these images arises from different heights of the oxide layer that grows on AlGaAs surfaces of different Al composition.[13] From such images, we conclude that the actual VQWR length is about 4.5 times the nominal thickness of the grown AlGaAs layer. This factor varies somewhat from sample to sample because of slightly accelerated growth rate along the wire axis. Using these measurements, we deduced the actual lengths L of VQWR1 in the grown samples, which range between ~9 and 630 nm. Transmission electron microscopy (TEM) images indicate that the width of VQWR1 is ~20 nm.[12] The effective Al contents (i.e., the ones that would yield an AlGaAs alloy of the same band gap as the segregated QWR) in each of the segregated regions can be determined with the aid of previous PL studies of similar pyramidal AlGaAs structures[12] and V-groove AlGaAs VQWs.[13] We thus estimated that the effective Al contents in the VQWR1, VQWR2, VQW1, and VQW2 are 4, 12, 17, and 37%, respectively. The resulting potential landscape of the pyramidal heterostructures considered here is depicted schematically in Figure 2, upper panel, where the colors, from red to

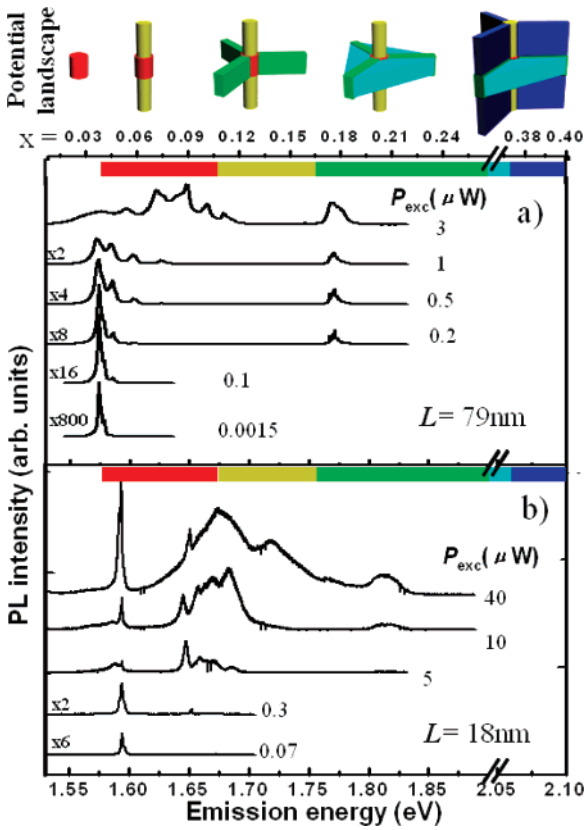

Figure 2. Top panel: Build-up of the potential landscape in an AlGaAs pyramidal structure with increasing energy/Al content, from left to right, showing the VQWR1, VQWR2, VQW1, $Al_{0.3}Ga_{0.7}As$ bulk, and VQW2 components. The indirect gap $Al_{0.55}Ga_{0.45}As$ bulk is omitted. Main part: two representative power dependence series of PL spectra of two samples with $L = 79$ nm (a) and $L = 18$ nm (b). The abscissa shows the photon energy (bottom scale) and the Al concentration x of the corresponding $Al_xGa_{1-x}As$ alloy (top scale). The horizontal color scale is correlated with the potential energy of the structures in the top panel, indicating the energy between the band gap of the corresponding structure and that of the next lowest band gap structure.

blue, correspond to an increasingly larger band gap and hence higher potential energy for carriers.

The samples were optically characterized by conventional micro-PL and polarization-resolved PL spectroscopy. They were mounted in a He-flow cryostat and kept at a constant temperature of $T = 10$ K. Single pyramids were excited nonresonantly by a Ar+ laser at a wavelength of 514 nm or by a frequency-doubled diode-pumped Nd:YVO_4 laser at a wavelength of 532 nm with a laser spot size of ~1 μm. The spectral resolution of the detection system was ~100 μeV. The PL spectra were measured either in top-view geometry, where the exciting beam and collected light propagated along the VQWRs, or in cleaved-edge geometry, where the beams propagated perpendicular to the axis of the VQWRs.

Figure 2a displays the micro-PL spectra of a single pyramid incorporating a VQWR1 structure of length $L =$ 79 nm, measured at different excitation levels. The origin of the observed transitions can be identified by referring to the potential landscape plotted at the upper panel of Figure 2. At the lowest excitation levels, the emission is due to recombination at the ground state of VQWR1 at

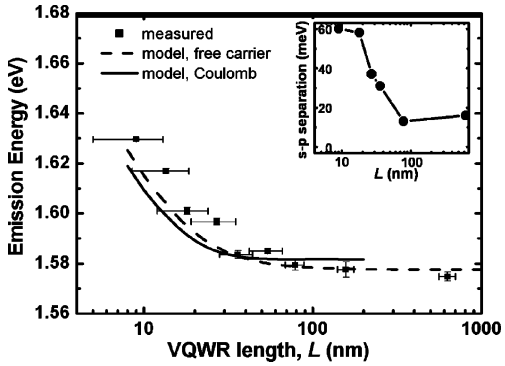

Figure 3. Main: measured ground-state transition energy versus VQWR1 length (squares). Dashed line represents the transition energies calculated by a free carrier model, then corrected by adding a constant exciton-binding energy 14.5 meV. Solid line shows the calculation accounting for the exciton-binding energies. Inset: measured energy separation of the ground and the first excited-state transitions as a function of VQWR1 length.

~1.575 eV. At higher excitation levels, transitions related to excited states of VQWR1 are also observed due to state-filling effects. The emission at ~1.775 eV is due to recombination at the VQW1. No emission from the cladding heterostructure (VQWR2 and VQW2) was observed at this excitation range, probably due to fast carrier transfer from those heterostructures to VQWR1 and VQW1.

For comparison, Figure 2b shows the power dependence spectra of a QD-like ($L \sim 18$ nm) sample. It can be seen that the ground-state transition is blue-shifted (by ~22 meV) as compared to that of the longer wire of $L = 79$ nm. Moreover, the spectra of the QD-like structure show only few emission peaks between the ground state and the energy corresponding to the lowest energy transition in the barrier, VQWR2 (broader peak at ~1.67 eV). These features are consistent with the additional confinement expected for sufficiently short VQWRs. In particular, for wire lengths comparable to its width, a QD structure should form; the spectra in Figure 2b are indeed similar to typical QD spectra, particularly at low excitation levels.

The complete trend of the variation in the measured transition energy as a function of wire length is presented in Figure 3 (squares). The vertical error bars indicate the full width at half-maximum (FWHM) of the corresponding emission peak. The horizontal error bars account for the error in determining the actual wire length due to possible growth rate variations along the axis of the pyramid. A monotonous increase in the ground-state transition energy with decreasing wire length is observed, although the increase becomes more abrupt for $L <$ ~30 nm. A similar trend of increase in the energy separating the ground and the first excited-state transition is also noticeable, as shown in the inset of Figure 2. Another clear trend we observed is the narrower line width of ground-state transitions for $L <$ ~30 nm, particularly at low excitation power; for example, for $L =$ 6 nm we measured FWHM ~ 300 μeV.

To gain insight into the role of quantum confinement effects on the evolution of the optical spectra, we used a model with simplified geometry to calculate the confined

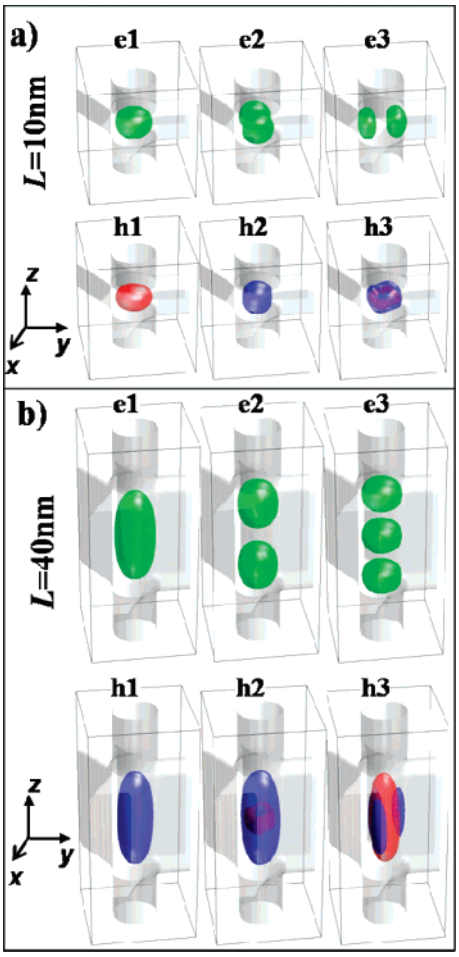

Figure 4. (color) Isosurfaces of computed probability distributions for the three lowest electron and hole states in VQWRs of length 10 nm (a) and 40 nm (b), corresponding to probability densities of 4×10^{-4} nm^{-3} and 1×10^{-4} nm^{-3}, respectively. The gray structures represent the shapes of the three lowest potential regions, corresponding to VQWR1, VQWR2, and VQW1 (see Figure 1). The electrons are represented by green, while the heavy and light components of the holes are represented by red and blue, respectively (see text for details).

states and the transition energies in these QWR/QD structures. The model system consists of three parallel layers of similar structures but different Al concentrations, corresponding to the core part and the two cladding regions. Each layer contains an $Al_xGa_{1-x}As$, [111]-oriented uniform cylinder of 16 nm diameter, representing the VQWR/QD, connected to three symmetrically arranged, 16 nm thick uniform $Al_yGa_{1-y}As$ slabs, representing the VQWs, all embedded in bulk $Al_zGa_{1-z}As$ (see gray areas in Figure 4). On the basis of our earlier studies of AlGaAs VQWRs,[12] we used $x = 2\%$, $y = 14.5\%$, and $z = 30\%$ for the core layer and $x = 9\%$, $y = 37\%$, and $z = 55\%$ for the cladding layers. The thickness of the core layer was varied to simulate the different values of the VQWR/QD length/thickness. The 3D problem was formulated in the effective mass approximation and was discretized by finite differences. A single band describes the electrons in the conduction band, while the holes in the valence band are described by a 4×4 Luttinger Hamiltonian[15] accounting for possible mixing between heavy and light holes. The interfaces between the grown layers are not abrupt on a nanometer scale; therefore, a 4 nm thick region of graded potential was introduced in the model at each interface.[16] To explore the impact of excitonic effects, the calculations were performed with and without the Coulomb interaction between the electrons and holes. In the former case, the exciton-binding energies were computed using a self-consistent Hartree approach.

The calculated variation of the ground-state transition (e_1-h_1) with VQWR length is shown in Figure 3. The dashed line shows the results obtained for free carriers (Coulomb interaction neglected), shifted down in energy by 14.5 meV for good fit with the experimental data. The value of 14.5 meV is interpreted as the average exciton-binding energy, and it agrees well with values reported for other QWRs of the same material system.[17] The solid line in Figure 3 represents the excitonic calculation without any adjustable parameter. Remarkable agreement is obtained between theory and experiments, demonstrating that the blue shift is indeed caused by additional quantum confinement along the axis of the VQWR for decreasing lengths. Note that the energy shifts with and without Coulomb interaction are comparable, indicating the onset of a strong quantum confinement regime in the vertical direction for the short VQWRs. In this QD regime, the model yields slightly lower transition energies than the measured ones as an effect of the simplified geometry used. In the real pyramidal geometry, the short VQWRs experience a higher potential due to the surrounding bulk AlGaAs. This effect is negligible for long VQWRs.

Figure 4 presents isosurfaces of the computed electron and hole probability density functions for the three lowest states in VQWRs of two different lengths, 10 and 40 nm, respectively. It can be seen that the excited-states electron wavefunctions, shown in green, primarily extend transversely for the 10 nm VQWR (Figure 4a) and longitudinally for the 40 nm VQWR (see Figure 4b), always corresponding to directions of weakest confinement. The two p-like states e_2 and e_3 for the 10 nm VQWR are degenerate, conforming to the C_{3v} symmetry of the structure potential.[18]

In contrast to the electron state, degeneracy does not apply to the hole states due to the presence of two hole types in this semiconductor. The heavy and light holes are distinguished by the angular momentum projection (J_z) on a quantization axis, chosen here as the z direction (i.e., the VQWR axis along [111]), for which $J_z = \pm 3/2$ and $J_z = \pm 1/2$, respectively. Note that the hole masses are anisotropic: a heavy (light) hole possesses a large (small) mass in the direction of quantization, but a small (large) mass in the perpendicular plane. For a system with 3D confinement, as studied here, the hole states are not expected to be purely "heavy" or "light" as for QWs; rather, a certain degree mixing occurs for each hole state. In Figure 4, the probability density distributions for the holes states are depicted as superposition of the heavy hole component (in red) and the light hole component (in blue). The hole ground states (h_1) for the 10 nm and the 40 nm VQWRs are very different, exhibiting predominantly heavy (87%) and light (94%) hole characters, respectively. The first excited state (h_2) has a switched character for the 10 nm VQWR and is strongly

(85%) of light hole character, while the corresponding hole state for the 40 nm VQWR remains predominantly light (86%) as the ground state. The second excited states (h_3) have transversely modulated wavefunctions and are of strongly mixed hole character for both VQWRs. Still, this state is mainly light (63%) for the 10 nm VQWR, but it switches character to become mainly heavy (64%) for the 40 nm VQWR.

The anisotropic hole masses yield interesting shapes of the probability density functions for the ground and excited state (h1 and h2) for the 10 nm VQWR. Because of the heavy hole character of the ground state, the large mass in the vertical direction results in strong confinement along *z*, while the small mass in the $x-y$ plane leads to lateral spreading. The situation is reversed for the excited state, which exhibits light hole character; it is elongated in the *z* direction, and the lateral spreading is reduced as compared to the ground state.

It is well known that the different hole characters are related to different polarization selection rules for optical transitions between the conduction band and the valence band.[19] Strongest difference in linear polarization is expected between pure heavy and light hole states, having the polarization vector oriented (mainly) parallel or perpendicular to the quantization axis, respectively. Different polarization dependence is therefore expected for VQWRs of different lengths exhibiting different hole characters (e.g., those of Figure 4). In search of such characteristics, which can serve as an indication of the carrier dimensionality, we performed polarization-resolved micro-PL spectroscopy on the series of VQWR samples discussed above. To allow access to linear polarization vectors oriented along, as well as perpendicular to, the VQWR, the luminescence was collected from the cleaved-edge of the sample (see Figure 5, upper part). The same experimental setup as for conventional PL was used, except that a linear polarizer was mounted in front of the entrance of the spectrometer at a fixed polarization direction, and the slow axis of a preceding $\lambda/2$-plate was rotated to resolve the linear polarization content of the detected PL signal.

Polarization-resolved PL spectra showing the lowest energy transitions, obtained for two samples of different lengths of VQWR1 ($L = 630$ nm and $L = 9$ nm) are shown in Figure 5 (lower part). Two closely spaced transitions are observed with weights that depend on the orientation of the polarization plane. The lower energy peak corresponds to the e_1-h_1 transition, whereas the higher energy peak is identified with the aid of our model as related to excited hole states, corresponding to e_1-h_3 (1D subbands) for $L = 630$ nm and e_1-h_2 (0D states) for $L = 9$ nm. The middle part in Figure 5 presents the computed dipolar matrix elements for parallel and perpendicular polarization vectors, above the corresponding spectra. For the QWR-like structure of $L = 630$ nm, the excited hole state (h_3) has a predominantly heavy-hole character, and thus it is essentially completely extinct for the parallel polarization direction (//). For the QD-like structure of $L = 9$ nm, as already discussed, the excited hole state (h_2) is expected to be

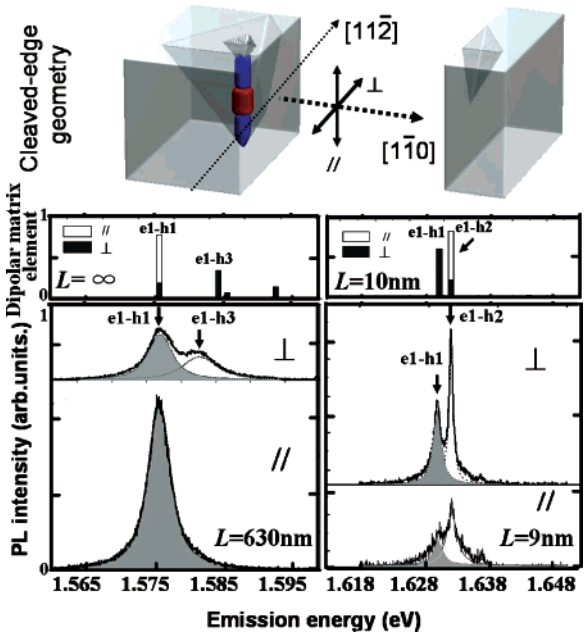

Figure 5. Top: sketch of cleaved-edge geometry used for measuring PL spectra for two different polarizations (⊥) and (//) with respect to the VQWR axis. Middle: computed dipolar matrix elements versus the transition energy, where a horizontal shift was introduced for exact match with the e1−h1 transition in the measured spectra shown below for convenient comparison. Bottom: PL spectra acquired from VQWR samples of different lengths, $L = 630$ nm (left) and $L = 9$ nm (right), with emission polarized perpendicular (upper panel) and parallel (bottom panel) to the wire axis. The filled regions show the Voigt fittings for the ground transition.

predominantly of light-hole character (see also Figure 4a), but the strong intensity detected for perpendicular polarization direction (⊥) suggests a mixed heavy- and light-hole character. For the other samples studied with intermediate VQWR1 length, the two transitions shown in Figure 5 were not well resolved, but the lowest energy peak shows a similar dependence on polarization as the e_1-h_1 transitions for $L = 630$ nm and $L = 9$ nm.

The full dependence of the polarization-resolved PL spectra on the length of VQWR1 is summarized in Figure 6, which depicts the degree of linear polarization $P \equiv (I_\perp - I_{//})/(I_\perp + I_{//})$ versus *L*, where $I_\perp$ ($I_{//}$) is the integrated intensity for light polarized perpendicular (parallel) to the VQWR axis for the lowest energy transition. For the VQWR1 lengths where the two lowest energy transitions were resolved, Voigt functions were used to fit the two line shapes (see Figure 5). When only one transition was resolved, the intensity of the full spectral line was evaluated. In Figure 6, the open circles show the results for several pyramidal structures characterized for each VQWR1 length, whereas the filled squares show the average measured values. The three VQWR samples with $L \geq 30$ nm show emission strongly polarized along the wire axis with $P \approx -0.6$, consistent with QWR-like polarization characteristics. For $L = 18$ nm, the samples still exhibit negative values of *P*, although reduced in magnitude. Finally, for the $L = 9$ nm sample positive values of the degree of polarization are

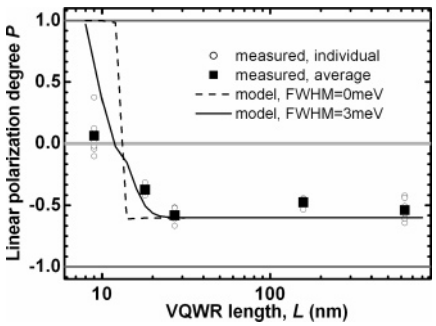

Figure 6. Degree of linear polarization P of the ground-state emission versus wire length. The open circles represent P measured from PL spectra whereas the filled squares represent the corresponding average values. The solid and dashed lines show the calculated P versus wire length with (FWHM = 3meV) and without broadening of the transitions involved, respectively.

observed, as large as $P = 0.375$ and with an average value of 0.061, indicating QD-like polarization characteristics.

The theoretical values of the degree of linear polarization were extracted from the abovementioned model by computing the dipolar matrix elements for the lowest energy transitions for polarization vectors parallel and perpendicular to the QWR axis. The results are shown in Figure 6 neglecting (dashed line) and including (solid line) spectral line broadening. The model calculations predict a rather abrupt switching from negative (QWR-like) to positive (QD-like) polarization anisotropy for wire lengths in the range 15−30 nm, that is, lengths comparable to the width of the VQWR potential well. The transition between the two regimes is made softer for finite (FWHM = 3 meV in this case) spectral linewidths, because the splitting between the heavy-hole and light-hole transition decreases near the switching length and thus merges the opposite behaviors of the two corresponding spectral lines. The calculated results accounting for the finite linewidths are in very good agreement with the measured ones. The spread in measured P values for each QWR/QD length, especially in the QD regime, probably reflects small variations in the aspect ratio of the QWR/QD involved. It is also interesting to note that the QWR length for which P changes from wire-like to dot-like depends quite sensitively on the assumed width of the VQWR. This can serve as another means for determining the QWR width in these structures. The assumed value of 16 nm is consistent with TEM measurements of similar structures;[11] however, the degree of linear polarization in the switching range of Figure 6 is much more sensitive to the value of the wire diameter as compared with the TEM data. Note also that both the polarization properties as well as the abrupt change in the ground-state energy (Figure 3) occur at wire lengths that are comparable to the exciton Bohr diameter. Hence, these effects correspond to the "strong" 3D confinement regime alluded to earlier.

The characteristics of optical polarization of semiconductor QWRs were studied by many groups both theoretically[20] and experimentally[21] using different model systems such as cylindrical, T-shaped, or V-grooved QWRs. The degree of linear polarization P for GaAs/AlGaAs QWRs, originating purely from 2D quantum confinement and consequent valence band mixing, has been predicted[20] and confirmed experimentally[21] to be ∼0.6. (Note that in previous studies the assignment of heavy and light hole masses refers to the direction of confinement[21] and not to the direction of free motion as in our case, because of different choice of the axis of quantization of the angular momentum.) Note that the strong polarization anisotropy ($P > 0.95$) related to electron−hole exchange exciton fine structure is not resolved in our experiments, due to very small splitting (∼100 μeV) of the exciton components in the present AlGaAs material. This is in contrast to in CdSe/ZnS nanorod systems, where the exciton fine structure splitting is significant (between 1.4 and 2.0 meV).[22] It should also be mentioned that the "giant" polarization anisotropy ($P \sim 0.96$) observed for nanowires,[23] arising from pure electromagnetic effects, can be excluded in our experiments. This giant anisotropy is observed for nanowires embedded in a medium having much lower refractive index than the wire's core. On the other hand, in the QWR structures discussed here the wire core and the surrounding media have similar refractive indices. This minimizes the impact of the electromagnetic effects and allows observation of the correlation between reduced carrier dimensionality and polarization anisotropy.

In summary, we have investigated the impact of dimensionality on several features of the optical spectra of semiconductor nanostructures, as their dimensionality is reduced from 1D (QWRs) to 0D (QDs). This was accomplished using a novel system of pyramidal nanostructures in which QWRs of specified length can be realized in a reproducible and reliable way. By systematically shrinking the length of the QWR, we observe the changes in the optical characteristics when the wires become sufficiently short, and in particular when their lengths are comparable or smaller than the exciton Bohr diameter. As expected, we observe increasing effective bandgaps and carrier state separations for decreasing wire length. Consistent with previous studies of "long" QWRs, we also observe the peculiar polarization anisotropy feature for luminescence from sufficiently long VQWRs. Interestingly, the switching from a QWR-like behavior to QD-like behavior observed in the features of the polarization anisotropy takes place for wires that are only 30 nm long. This explains the QWR-like features of polarization anisotropy exhibited by many experimental QWR systems, although they all suffer from certain degrees of carrier localization, sometimes refered to as "QD behavior", due to wire imperfections.

The ability to control the optical polarization characteristics of QWR/QD systems has potential applications in many photonic devices in which the polarization features of the light source need to be matched to those of an optical waveguide or cavity, for example, semiconductor lasers or photonic crystal devices. Moreover, the pyramidal QWR/QD system provides considerable freedom in designing and realizing complex wire/dot nanostructures that are difficult to achieve with purely self-assembly approaches, for example, QD molecules and QD superlattices with controlled size and potential profiles.

References

(1) (a) Jaskólski, W. *Phys. Rep.* **1996**, *271*, 1. (b) Bimberg, D.; Grundmann, M.; Ledentsov, N. N. *Quantum Dot Heterostructures*; John Wiley & Sons: New York, 1999. (c) Michler, P. *Single Quantum Dots: Fundamentals, Applications and New Concepts (Topics in Applied Physics)*; Springer: New York, 2004.

(2) (a) Vouilloz, F.; Oberli, D. Y.; Dupertuis, M.-A.; Gustafsson, A.; Reinhardt, F.; Kapon, E. *Phys. Rev. Lett.* **1997**, *78*, 1580. (b) Goldoni, G.; Rossi, F.; Molinari, E.; Fasolino, A. *Phys. Rev. B* **1997**, *55*, 7110.

(3) (a) Citrin, D. S. *Phys. Rev. Lett*, **1992**, *69*, 3393. (b) Heitz, R.; Veit, M.; Ledentsov, N. N.; Hoffmann, A.; Bimberg, D.; Ustinov, V. M.; Kop'ev, P. S.; Alferov, Zh. I. *Phys. Rev. B*, **1997**, *56*, 10435. (c) Oberli, D. Y.; Dupertuis, M.-A.; Reinhardt, F.; Kapon, E. *Phys. Rev. B* **1999**, *59*, 2910.

(4) (a) Akiyama, H. *J. Phys.: Condens. Matter*, **1998**, *10*, 3095. (b) Hartmann, A.; Ducommun, Y.; Kapon, E.; Hohenester, U.; Molinari, E. *Phys. Rev. Lett.* **2000**, *84*, 5648. (c) Crottini, A.; Staehlia, J. L.; Deveaud, B.; Wang, X. L.; Ogura, M. *Solid State Comm.* **2002**, *121*, 401.

(5) Vouilloz, F.; Oberli, D. Y.; Dwir, B.; Reinhardt, F.; Kapon, E. *Solid State Comm.* **1998**, *108*, 945.

(6) (a) Akiyama, H.; Pfeiffer, L. N.; Pinczuk, A.; West, K. W.; Yoshita, M. *Solid State Comm.* **2002**, *122*, 169. (b) Ambigapathy, R.; Bar-Joseph, I.; Oberli, D. Y.; Haacke, S.; Brasil, M. J.; Reinhardt, F.; Kapon, E.; Deveaud, B. *Phys. Rev. Lett.* **1997**, *78*, 3579.

(7) (a) Bellessa, J.; Voliotis, V.; Grousson, R.; Wang, X. L.; Ogura, M.; Matsuhata, H. *Appl. Phys. Lett.* **1997**, *71*, 2481. (b) Malko, A.; Baier, M. H.; Pelucchi, E.; Oberli, D. Y.; Leifer, K.; Chek-al-kar, D.; Kapon, E. *Appl. Phys. Lett.* **2004**, *85*, 5715. (c) Otterburg, T.; Oberli, D. Y.; Dupertuis, M. A.; Moret, N.; Pelucchi, E.; Dwir, B.; Leifer, K.; Kapon, E. *Phys. Rev. B* **2003**, *71*, 033301. (d) Hess, H. F.; Betzig, E.; Harris, T. D.; Pfeiffer, L. N.; West, K. W. *Science* **1994**, *264*, 1740.

(8) Guillet, T.; Grousson, R.; Voliotis, V.; Wang. X. L.; Ogura, M. *Phys. Rev. B* **2003**, *68*, 045319.

(9) Schedelbeck, G.; Wegscheider, W.; Bichler, M.; Abstreiter, G. *Science*, **1997**, *278*, 1792.

(10) (a) Sköld, N.; Karlsson, L. S.; Larsson, M. W.; Pistol, M.-E.; Seifert, W.; Trägärdh, J.; Samuelson, L. *Nano Lett.* **2005**, *5*, 1943. (b) Borgström, M. T.; Zwiller, V.; Muller, E.; Imamoglu, A. *Nano Lett.* **2005**, *5*, 1439.

(11) Hartmann, A.; Ducommun, Y.; Leifer, K.; Kapon, E. *J. Phys.: Condens. Matter* **1999**, *11*, 5901.

(12) Zhu, Q.; Pelucchi, E.; Dalessi, S.; Leifer, K.; Dupertuis, M.-A.; Kapon, E. *Nano Lett.* **2006**, *6*, 1036.

(13) Reinhardt, F.; Dwir, B.; Biasiol, G.; Kapon, E. *Appl. Phys. Lett.* **1996**, *68*, 3168.

(14) Biasiol, G.; Reinhardt, F.; Gustafsson, A.; Martinet, E.; Kapon, E. *Appl. Phys. Lett.* **1996**, *69*, 2710.

(15) (a) Luttinger, J. M.; Kohn, M. *Phys. Rev.* **1955**, *97*, 869. (b) Luttinger, J. M. *Phys. Rev.* **1956**, *102*, 1030.

(16) Biasiol, G.; Martinet, E.; Reinhardt, F.; Gustafsson, A.; Kapon, E. *J. Cryst. Growth*, **1997**, *170*, 600.

(17) (a) Dupertuis, M.A.; Oberli, D.Y.; Kapon, E. In *Proceedings of ICCN 2002*; Computational Publications: Cambridge, MA, 2002; p 227. (b) Gammon, D.; Snow, E. S.; Shanabrook, B. V.; Katzer, D. S.; Park, D. *Phys. Rev. Lett.* **1996**, *76*, 3005.

(18) Michelini, F.; Dupertuis, M.-A.; Kapon, E. *Appl. Phys. Lett.* **2004**, *84*, 4086.

(19) Bastard, G. *Wave Mechanics Applied to Semiconductor Heterostructures*; Les Editions de Physique: Les Ulis, France, 1988.

(20) (a) Bockelmann, U.; Bastard, G. *Phys. Rev. B* **1992**, *45*, 1688. (b) Sercel, P. C.; Vahala, K. J. *Phys. Rev. B* **1991**, *44*, 5681.

(21) (a) Vouilloz, F.; Oberli, D. Y.; Dupertuis, M.-A.; Gustafsson, A.; Reinhardt, F.; Kapon, E. *Phys. Rev. B*, **1998**, *57*, 12378. (b) Itoh, H.; Hayamizu, Y.; Yoshita, M.; Akiyama, H.; Pfeiffer, L. N.; West, K. W.; Szymanska, M. H.; Littlewood, P. B. *Appl. Phys. Lett.* **2003**, *83*, 2043.

(22) Thomas, N. Le.; Herz, E.; Schöps, O.; Woggon, U.; Artemyev, M. V. *Phys. Rev. Lett.* **2005**, *94*, 016803.

(23) Wang, J. F.; Gudiksen, M. S.; Duan, X. F.; Cui, Y.; Lieber, C. M. *Science* **2001**, *293*, 1455.

NL0706650